DEUTSCHES ELEKTRONEN – SYNCHROTRON

DESY 91-006
February 1991

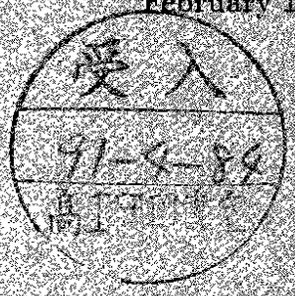

Studies of Multihadronic Final States in Photon-Photon Interactions

CELLO Collaboration

ISSN 0418-9833

NOTKESTRASSE 85 · D-2000 HAMBURG 52

To be sure that your preprints are promptly included in the HIGH ENERGY PHYSICS INDEX, send them to the following (if possible by air mail):

DESY
Bibliothek
Notkestrasse 85
D-2000 Hamburg 52
Germany

DESY 91-006
February 1991

ISSN 0418-9833

STUDIES OF MULTIHADRONIC FINAL STATES IN PHOTON-PHOTON INTERACTIONS.

CELLO Collaboration

H.-J. Behrend, L. Criegee, J.H. Field[1], G. Franke, H. Jung[2],
J. Meyer, O. Podobrin, V. Schröder, G.G. Winter
Deutsches Elektronen-Synchrotron, DESY, Hamburg, Germany

P.J. Bussey, A.J. Campbell, D. Hendry, S.J. Lumsdon, I.O. Skillicorn
University of Glasgow, United Kingdom

J. Ahme, V. Blobel, M. Feindt, H. Fenner,
J. Harjes, J.H. Köhne[3], J.H. Peters, H. Spitzer, T. Weihrich
II. Institut für Experimentalphysik, Universität Hamburg, Germany

W.-D. Apel, J. Engler, G. Flügge[2], D.C. Fries, J. Fuster[4], K. Gamerdinger[5],
P. Grosse-Wiesmann[6], H. Küster[7], H. Müller, K.H. Ranitzsch, H. Schneider
Kernforschungszentrum Karlsruhe und Universität Karlsruhe, Germany

W. de Boer[3], G. Buschhorn, G. Grindhammer, B. Gunderson, C. Kiesling, R. Kotthaus,
H. Kroha[8], D. Lüers, H. Oberlack, P. Schacht, S. Scholz, W. Wiedenmann[6]
Max Planck-Institut für Physik und Astrophysik, München, Germany

M. Davier, J.F. Grivaz, J. Haissinski,
V. Journé, F. Le Diberder[9], J.-J. Veillet
Laboratoire de l'Accélérateur Linéaire, Orsay, France

K. Blohm, R. George, M. Goldberg, O. Hamon, F. Kapusta, L. Poggioli, M. Rivoal
Laboratoire de Physique Nucléaire et des Hautes Energies,
Université de Paris, France

G. d'Agostini, F. Ferrarotto, M. Iacovacci, G. Shooshtari, B. Stella
University of Rome and INFN, Italy

G. Cozzika, Y. Ducros,
Centre d'Etudes Nucléaires, Saclay, France

G. Alexander, A. Beck, G. Bella, J. Grunhaus, A. Klatchko [10], A. Levy, C. Milstène
Tel Aviv University, Israel

[1]Now at Université de Genève, Switzerland
[2]Now at RWTH, Aachen, Germany
[3]Now at Univ. Karlsruhe, Germany
[4]Now at Inst. de Física Corpuscular, Universidad de Valencia, Spain
[5]Now at MPI für Physik und Astrophysik, München, Germany
[6]Now at CERN, Geneva, Switzerland
[7]Now at DESY, Hamburg, Germany
[8]Now at Univ. of Rochester, USA
[9]Now at Stanford Linear Accelerator Center, USA
[10]Now at University of California, Riverside, USA

Abstract

We have measured the cross section and Q^2-dependence of the reaction $\gamma\gamma \rightarrow$ multihadrons, using the CELLO detector at DESY, for visible final-state masses between 4 and 9 GeV. The data are well fitted by an incoherent sum of Generalised Vector Meson Dominance and Quark Parton Model terms, but at low Q^2 require the addition of a third component which resembles the QPM but is less two-jet-like. With and without this term, the GVDM cross section at Q^2=0 is found to be 200 ± 20 and 250 ± 25 nb, respectively.

1. Introduction.

In this paper we describe a study by the CELLO collaboration of the production of multihadronic events in photon-photon interactions. These represent an important class of processes which occur alongside annihilation reactions in e^+e^- collisions. In the reaction

$$e^+e^- \rightarrow e^+e^-X,$$

each of the beam leptons radiates a virtual photon; these then interact to give the observed final state. Averaged over virtual photon polarisations, the cross section for this process depends on the invariant mass W of the photon-photon system and the invariant masses of the virtual photons. These are each emitted with an approximate bremsstrahlung spectrum, whose intensity also varies with the virtual photon mass squared Q^2 as $1/Q^2$. When a virtual photon is radiated at a substantial value of Q^2, the beam lepton may be deflected through a sufficiently large angle to be detected. This "tags" the virtual photon, enabling its energy and Q^2 value to be measured. In practice, events with two tags are very rare. Here we analyse a data sample consisting of untagged and single-tagged events.

Previous experiments [1, 2, 3] have established the existence of at least two components in the process

$$\gamma\gamma \rightarrow hadrons$$

at W values above a few GeV. For events at low Q^2, and whose tracks have low average momentum p_t transverse to the beam line, the reaction appears to be dominated by non-perturbative processes, which can be represented in a natural way by the vector meson dominance model. Of the various forms of this, the Generalised Vector Meson Dominance Model (GVDM) was found by PLUTO [1, 2] to be the most successful, although the TPC/2γ collaboration [3] favoured other forms. The total cross section is consistent with being constant in W for W greater than a few GeV, but falls rapidly with Q^2. At large values of Q^2 or p_t, a point-like component becomes increasingly important. This is well described by the Quark Parton Model (QPM) (fig. 1). In addition, the presence of a third component to the cross section at low Q^2 and medium p_t was reported by PLUTO [2].

The purpose of the present work will be to examine whether the CELLO data are also described by these models, and to evaluate the photon-photon hadronic cross section.

2. Theoretical Models.

The various forms of the vector meson dominance model parameterise the total cross section in the form

$$\sigma_{\gamma\gamma} = \sigma(W)\, F(Q_1^2)\, F(Q_2^2),$$

where $F(Q^2)$ represents a form factor. In GVDM, the form factor includes pole terms from the ρ, ω and ϕ vector mesons, and also a continuum term:

$$F_{GVDM} = \sum_{v=\rho,\omega,\phi} r_v \frac{1+\frac{Q^2}{4m_v^2}}{(1+\frac{Q^2}{m_v^2})^2} + \frac{0.22}{(1+\frac{Q^2}{m_0^2})}$$

As in [1], the values used for the ρ, ω and ϕ masses m_v and coupling ratios r_v are respectively $m_v = 0.769, 0.783, 1.020$ GeV and $r_v = 0.65, 0.08, 0.05$; $m_0 = 1.4$ GeV. Other forms of the model omit the continuum term, or in the simplest case retain just a ρ pole term, with suitable renormalisation of the coupling ratios.

A different approach is taken by Gotsman, Levy and Maor (GLM) [4], who parameterise a variety of existing data in a form that incorporates Bjorken scaling at high Q^2, and suitable threshold factors. A QPM term is added. Photon structure functions from previous measurements at PETRA are used, together with data from Novosibirsk. A comparison with this model therefore in part indicates whether our present results are consistent with previous work. This model gives fixed predictions with no free parameters.

The cross section for the process $\gamma\gamma \to q\bar{q}$ is similar to that for $\gamma\gamma \to \mu\mu$ [5], but with a factor $3\epsilon^4$ where ϵ is the quark charge and the factor 3 allows for colour. It is summed over all quark pairs allowed at a given W value, to give the Quark Parton Model. The cross section peaks at W values around three times the quark mass, and for large W and Q^2 varies approximately as $1/(W^2+Q^2)$. It may be noted that the QPM cross section is dominated by the charge $\frac{2}{3}$ quarks, namely u and c, but that the contribution of the charm quark is depressed at the W values typical of the present experiment, owing to its relatively high mass. At W=5 GeV and Q^2=0, using u, d, s, c quark masses of 0.3, 0.3, 0.5, 1.5 GeV, the QPM total cross section is 43.3 nb, of which 29.0 and 10.9 nb respectively come from the u and c quarks.

The basic QPM process may be augmented by related higher order processes. The cross section for the process $\gamma\gamma \to gg$ via quark box diagrams has been evaluated to be 8–20% of the QPM cross section [6]. Brodsky et al.[7] have presented studies of those diagrams in which the presence of hard scattering subprocesses allows a perturbative approach to be used. They predict that three- and four-jet events will occur at levels which can rise to several times the 2-jet (i.e. QPM) cross section for events with soft jets along the beam axis. (The latter jets may not be easily identified in practice, however.) Excesses over QPM of up to ~50% are predicted for our acceptance, although in view of the simplifications made, these figures should probably be regarded as rough estimates. In our present analysis, a simple model for three- and four-jet production was considered. Details of it are given in [2].

It has been a matter of frequent debate whether the QPM contributes to the GVDM term or is independent of it. Since the Q^2 and W dependences of the two terms are very different, the former would appear unlikely, at least with the constant form usually taken for $\sigma(W)$ in GVDM. A small perturbative term can of course always exist alongside a large non-perturbative term, although interference effects may be present. In what follows, our approach is to attempt a phenomenological fit of the data to the various models, ignoring interference effects. It will be shown that the presence of a third contribution to the Q^2=0 cross section is indicated, and that this can be distinguished from both the GVDM term and the QPM term.

In the following analysis, events from Monte Carlo event generators were passed through a standard CELLO apparatus simulation, before being subjected to the same analysis programs as the data. Monte Carlo luminosities of 180 pb^{-1} were generated for each model, the statistics being limited by the large quantities of computer time required. The statistical errors on the Monte Carlo data were taken into account in evaluating χ^2 values of fits. The QPM events were simulated using a generator of Daverveldt [8], the $q\bar{q}$ pairs being subjected to Lund 7.2 fragmentation.

The GVDM generator is more phenomenological in nature. A primary quark pair of given W value is generated with a transverse momentum distribution relative to the beam direction of $exp(-5p_t^2)$. The quarks are then fragmented using the non-standard parameter σ=450 MeV instead of the more normal value of 350 MeV [2]. This parameterisation was found by PLUTO to work well, and effectively represents the ρ meson as having a broader fragmentation than quarks. It was confirmed by an investigation that the results are insensitive to whether Feynman-Field or Lund fragmentation is used.

3. Apparatus and event selection.

The data used in the present analysis were taken in 1986 with the CELLO detector at PETRA, DESY, with an integrated luminosity of 86 pb^{-1}. The energy of each beam was 17.5 GeV. Full details of CELLO have been given elsewhere [9]. The principal features of relevance to the present analysis are:

1. The central tracker, which consisted of 14 interleaved cylindrical drift chambers and proportional chambers. A magnetic field of 1.3 Tesla was provided by a superconducting solenoid. With vertex constraint, charged tracks could be measured with a momentum resolution of 1.2% (GeV/c)$^{-1}$. The acceptance was 97% of 4π. Measurements of z to $\pm 440\mu$m per point were made on cathode strips in the five proportional chambers.
2. The lead liquid argon calorimeter. This was divided into a barrel section and two endcaps, each approximately 20 radiation lengths deep. In the barrel, electromagnetic showers were recorded with an energy resolution of $\pm 10\%/\sqrt{E(\mathrm{GeV})} \pm 5\%$, and an angular resolution of ± 3 mrad. The angular acceptance was 87% of 4π. The endcaps were used as a tagging device rather than as a photon detector, for tags between 150 and 360 mrad. Thus the acceptances for charged tracks and photons were roughly matched.
3. The forward detectors. These consisted of arrays of lead glass blocks, with semicircular scintillator strips in front. They detected tags between 40 and 100 mrad, with an energy resolution of $\pm 10\%/\sqrt{E(\mathrm{GeV})}$ and a polar angle resolution of ± 3 mrad. In the present measurements, only the region 55–80 mrad was used where the calibration was best.

Trigger signals were obtained from various parts of the apparatus and combined in two Master Trigger Units, which selected the chosen combinations of signals. Of particular importance for the present data were triggers which required one or more of the following conditions:

1. At least two tracks with transverse momentum $p_t > 650$ MeV/c and an opening angle $> 135^0$ in ϕ, with at least one track pointing to the interaction point in rz.
2. As (1), but with the opening angle requirement replaced by limits on the numbers of

hits in the inner chambers in the central tracker, to reduce beam-pipe background.

3. As (1), but with the lower p_t limit reduced to 250 MeV/c, and both an opening angle requirement and limits on the inner chamber hits.
4. 2 GeV in a forward detector plus (a) a track with $p_t > 250$ MeV/c and a signal from a track pointing to the interaction point in rz, or (b) an energy deposit of >800 MeV in a barrel liquid argon module.
5. As (4), but with the forward detector requirement replaced by a requirement for at least 1.5 GeV recorded in an endcap module.

The events were passed through a filter program which confirmed presence of the claimed trigger conditions, before being accepted for full processing. Track reconstruction and shower reconstruction in the liquid argon were then performed, allowing the selection of broad classes of physically interesting events. There followed a more detailed reconstruction of liquid argon showers, quality checks on the charged tracks, V^0 reconstruction and identification of tags. Electrons above a few hundred MeV could now be identified by their shower characteristics in the liquid argon.

The main requirements for the event selection for the present analysis were:

1. A least four charged tracks, with overall charge imbalance ≤ 2.
2. Overall transverse momentum imbalance ≤ 3 GeV/c (including any detected tag).
3. The measured point of origin of the event along the beam line was required to be within ± 4 cm of the interaction point.
4. The observed mass W_{vis} of the accepted charged and neutral tracks within the limits $4 \leq W_{vis} \leq 9$ GeV.
5. For tagged events, the reconstructed missing momentum along the beam axis of the entire event (including the tag) had to exceed 8 GeV/c.

In applying the above cuts, the following conditions were applied to the tracks, rejected tracks being ignored:

- $|\cos\theta| \leq 0.95(0.85)$ for charged (neutral) tracks; this confined the charged tracks to the best measured region and demanded that neutral tracks lay within the barrel calorimeter.
- Charged tracks were required to approach the interaction point to within 10 mm in $r\phi$.
- Charged track momenta above 5 GeV/c were reset to 5 GeV/c to reduce the effects of measurement errors.
- Showers within 4 mrad of the edge of a liquid argon module were rejected.
- Showers of energy less than 200 MeV were rejected.

Badly measured events were reduced mainly by cuts (1) and (2), beam gas background by cuts (1)–(3), and annihilation background by cuts (2), (4) and (5). After the cuts, the numbers of untagged, forward-tagged and endcap-tagged events obtained are listed in table 1.

4. Backgrounds.

Backgrounds to the process $\gamma\gamma \to$ *multihadrons* arise from a variety of sources. We

list the following, and their treatment:

(1) Beam-gas and beam-pipe collisions. These processes are characterised by multiple soft positively-charged tracks, and have vertices distributed uniformly along the beam axis z. However it was found that after the reconstruction and selection of the events, the remaining background vertices peaked somewhat around $z = 0$, making their subtraction problematic. Data taken with the electron and positron beams laterally separated were used to investigate this effect. It was concluded that events whose vertex lay between 4–8 cm from the interaction point should be subtracted as a sideband from the main sample, but with a weight of 2.0. This was a 3% correction to the data.

(2) e^+e^- annihilation. This formed the largest single source of background. Events with initial-state radiation or much missing energy can resemble photon-photon events, and high-energy, low angle π^0s can also simulate tags. The process was simulated using a standard generator with initial-state radiation and Lund 6.3 fragmentation; the events were passed through a detector simulation and the same selection cuts as the data. The resulting W_{vis} distribution is shown in fig. 2. The background varies from 5% of the total events at $W_{vis} = 4$ GeV to approximately 50% at 9 GeV. It is found to have flat distributions in thrust and p_t^{jet} (c.f. section 6); all events with $p_t^{jet} > 4$ GeV/c were consistent with being annihilation background, and the background represents around 35% of the total data for $2 < p_t^{jet} < 3$ GeV/c. The error bars in the plots of these quantities take the background subtraction into account.

(3) τ pair production. The processes $e^+e^- \to \tau^+\tau^-$ and $\gamma\gamma \to \tau^+\tau^-$ give rise to multiparticle final states for which our event selections have some acceptance. They were simulated and found to give rise to negligible corrections of less than 1%.

5. Thrust Analysis.

In order to obtain a more detailed description of the structure of the events, a thrust analysis was performed. For each event, the thrust T is defined as the maximum value taken by the quantity

$$\frac{\sum |\mathbf{p}_i.\mathbf{n}^{jet}|}{\sum |\mathbf{p}_i|}$$

where each sum is over the charged and neutral tracks in the event, and $\mathbf{n}^{jet}$ is a unit vector called the jet axis, whose direction is varied to maximise T. This divides the particles in each event into two "jets", consisting of those groups of tracks for which $\mathbf{p}_i.\mathbf{n}^{jet}$ is positive or negative respectively. We allow a single charged or neutral track to constitute a jet. T=0.5 represents a completely "spherical" event, T=1 a perfectly collimated two-jet event. Thrust is used here in preference to other event-shape variables since it is relatively insensitive to the presence of decaying resonances in the final state. The analysis is performed in the centre of mass system of the observed tracks, which involves boosting all tracks along a direction θ_{boost} relative to the e^+e^- axis. For each jet we evaluate p_t^{jet} as $|\mathbf{p}^{jet}| \sin\theta^{jet}$, where $\mathbf{p}^{jet}$ is the total momentum of the tracks in each jet, and θ^{jet} is the angle between the jet axis and the $\gamma\gamma$ axis. For untagged events, the $\gamma\gamma$ axis in the c.m. system is taken to be at an angle $-\theta_{boost}$ to the direction of the c.m. boost. For tagged events, the interacting photon which was reconstructed from the tag is boosted into the c.m. system where it defines the $\gamma\gamma$ axis.

The relationship between the jet axis and the underlying physics of the event varies according to the nature of the latter. A "spherical" event — e.g. governed by phase space — will have an essentially random jet axis. The reconstructed jet axis of a QPM event

before the tracks pass through the detector simulation reflects the angle of the parton typically to within $\pm 7^0$. This agreement is degraded by typically $\pm 10^0$ after reconstruction in the detector, although for some poorly measured events the effect is larger.

The acceptance of the apparatus has a marked effect on the measured thrust of an event. Particles produced at small angles to the beam remain unmeasured; hence their contribution to the thrust will be absent. GVDM events are typically p_t-limited with a high thrust along the beam direction. Their measured thrust will therefore be less than its true value. On the other hand, spherical events will have portions missing in the $\pm z$ directions so as to give a measured thrust which is too high. Despite this, it will be seen that the thrust as measured by CELLO gives a useful key to the nature and shape of photon-photon events.

6. The Untagged Data.

Some general features of the data are given in figs 3-6(a). All data points are fully background-subtracted, and all Monte Carlo data has been fully passed through the detector simulation. Suffix t refers to transverse momentum components relative to the $\gamma\gamma$ axis in the c.m. system of the observed final state. The dashed histograms represent the distribution expected for a model consisting of a GVDM term with a flat cross section in W, and a QPM term. The QPM term is fixed at the standard cross section, while the GVDM term is normalised to make the total numbers of events agree with the data. For the untagged data we observe the following features:
(1) The W_{vis} distribution (fig. 3) is well fitted by the sum of GVDM+QPM, but the data suggest a slightly slower fall-off with W_{vis}.
(2) The p_t distribution for individual particles shows an excess which develops above a value of 1 GeV/c (fig. 4).
(3) The p_t^{jet} distribution (fig. 5) shows an excess of jets with $p_t > 1.5$ GeV/c.
(4) There is an excess of wide-angle jets. (Fig. 6; the apparent deficit of small-angle jets is due to the normalisation of the Monte Carlo to the event sample.)

It should be noted that the observed excesses are found particularly in those kinematic regions where the GVDM term is relatively small (fig. 7). They cannot therefore be removed by renormalising the GVDM term, nor can they easily be attributed to interference effects involving the GVDM term.

One potential cause of discrepancies which was investigated was the possible mismeasurement of charged tracks and showers: the false assignment of a high momentum to even a small fraction of tracks might distort the upper ends of the p_t distributions considerably. The limit on measured track momenta of 5 GeV/c greatly reduces this source of background. We also tested the effect of tightening the angular cuts on the charged tracks from $\cos\theta$=0.95 to $\cos\theta$=0.90, these being the least well measured tracks. The minimum photon energy was also raised from 200 to 300 MeV, although this change would not be expected to have much effect on high p_t^{jet} events. It was found that these modifications had little effect on the p_t characteristics of the events, or on their thrust distributions. The numbers of events were reduced to 60% of the full statistics, however, with the background fraction rising from 12% to 18%. (As expected, the biggest reduction was in the numbers of events at lower θ^{jet} values, e.g. $\theta^{jet} < 40^0$ — a class of events dominated by GVDM processes.) In short, the events which give rise to the high-p_t excesses appear to be among our better measured events, confirming that an interpretation must be sought in terms of physical processes additional to GVDM and QPM.

Three additional types of process were investigated (the full data sample being retained throughout):

1. An additional QPM component obtained by scaling up the standard term.
2. An all-pion phase-space component with (a) constant cross section in W, (b) cross section varying as $1/W^2$ to resemble a QPM-like cross section.
3. QPM-like processes modified to have additional parton jets. Three- and four- jet processes are generated as in [2]. This is an oversimplification of the higher order processes, but should give a rough indication of their properties.

The fraction of the extra component was varied to minimise χ^2 for the p_t^{jet} histogram. It was found that terms of type (1), (2a) and (2b) were able to improve the p_t^{jet} distributions considerably. Fig. 8 (for (2a); (2b) is similar) shows typical results. However the processes of type (3) fitted the high-p_t^{jet} points only at the expense of generating many low-pt tracks and jets. The p_t^{jet} fit required $41 \pm 5\%$ of the GVDM to be replaced by the 3-jet term, or $92 \pm 8\%$ of it to be replaced by the 4-jet term. The fits are poor ($\chi^2/d.f. = 12.1, 16.3$ respectively). These cross sections are in conflict with the GVDM cross sections found for the tagged data (see next section), and in the 4- jet case are very much higher than expected theoretically [7]. None of this seems physically reasonable.

Further information on the nature of the third component is obtained from its thrust characteristics. The overall thrust distribution of the events is given in fig. 9, showing that the additional component must be measured in CELLO to have higher thrust than the average untagged event. This appears to contradict the result of PLUTO, where a lower-thrust component was required; however it should be remembered that the PLUTO forward spectrometers were able to measure well the high thrust of the low θ^{jet} GVDM component, which is unmeasured or truncated to lower measured thrust in CELLO. Events with $p_t^{jet} > 2$ GeV were now selected. Their thrust distribution is compared with GVDM+QPM in fig. 10 in the absence of a third component.

When the fitted quantities of models (1) and (2) are included, the thrust distributions shown in fig. 11, are obtained. It is evident that an event shape intermediate between the QPM and phase space models is required. Some general characteristics of the fits are listed in table 2. The χ^2 values include the contributions from the statistical errors in the Monte Carlo data. It is apparent that even the best fits to W_{vis} and p_t^{jet} are mediocre on the basis of χ^2 alone. Systematic effects of the order of ten percent would be sufficient to cover the remaining discrepancies in the W_{vis} plot for the high-p_t^{jet} events; meanwhile it is evident from this and the p_t^{jet} distribution (which is correlated with W_{vis}) that a $1/W^2$ dependent cross section for the third term is preferred over a flat cross section. (A $1/W$ dependence gives intermediate χ^2 values.) In general, the remaining discrepancies are of a magnitude which is compatible with the poor description of the event shapes by the models used. (A tuned mixture of phase-space/W^2 and QPM was found to be capable of describing all the distributions well, at the expense of being physically somewhat artificial.)

In view of the claim by TASSO [10] that the charm content of photon-photon events is much higher than expected, we ask whether the excess observed in our data is attributable to this cause. (TPC/2γ, however, report a charm cross section compatible with the QPM expectation [11].) Instead of rescaling the QPM component as a whole, the p_t^{jet} distribution can be fitted by rescaling just the charm component by a factor of 3.8. This gives a $\gamma\gamma \to c\bar{c}$ cross section of around 50 nb at the lower end of our W range,

still much less than TASSO's estimate of 141 nb (which could, of course, have sources other than a QPM-like term). Further information comes from the observed inclusive K_s^0 rate. We observe 36 inclusive K_s^0 in our events with $2 < p_t < 4$ GeV, compared with a QPM expectation of 29. (The GVDM contribution is believed to be small in this range.) Rescaling the $\gamma\gamma \to c\bar{c}$ cross section by 3.8 increases this number to 79, in disagreement with the data. Even scaling up the QPM contribution as a whole as in fit (1) is barely compatible with the observed K_s^0 rate.

The high-p_t component of the 3- and 4- jet models considered, however, gave a good fit to the observed thrust distribution ($\chi^2/d.f. = 4.0, 2.0$, respectively), despite the poor performance of these models overall. It would appear, therefore, that the observed excess over GVDM+QPM points to a QPM-like process whose emerging quarks have a broader fragmentation than QPM, possibly due to higher order QCD effects, but with a different low-p_t spectator-quark component from the multijet models considered. We note that the third component required by PLUTO could be represented as phase-space/W^2 with a magnitude approximately equal to that of the QPM term. This is consistent with the results above.

The χ^2 for the W_{vis} distribution of the entire sample of 15k events is around 2.0 per degree of freedom when models (1) or (2b) are used, well within the systematic uncertainties on the measurements. This confirms that a flat GVDM cross section gives an excellent description of the data over the W range that gives rise to the W_{vis} values observed. We therefore evaluate a single cross section value, which will be presented below, for the GVDM component. An alternative procedure is to unfold the various effects that move W to different W_{vis} values and present a series of W-dependent cross sections. However in view of the complexity and model-dependence of the unfolding procedure, and the risk of introducing further systematic errors, we have chosen not to do this since it appears unnecessary in the present analysis.

To estimate the systematic errors on the results due to uncertainties on detector effects, fragmentation, etc., a variety of kinematic variables were plotted and compared with the best model fits (e.g. charged and neutral multiplicities, angular distributions, etc.) Discrepancies of a few percent are typical. Further contributions are 3% from the beam luminosity and 3% from background subtractions overall. The model dependence of the third term and the error on the annihilation background each introduce uncertainties of about 10% on its magnitude. The overall systematic error on the GVDM cross sections is estimated as $\pm 10\%$.

7. The Tagged Data.

Similar jet analyses were performed for the tagged data as for the untagged; the W_{vis}, p_t p_t^{jet} and θ^{jet} distributions are shown in figs 3–6(b,c). A model comprising varying amounts of GVDM and a standard QPM component was fitted to the numbers of events in each tagging region; fig. 12 shows the resulting Q^2 distributions. Although fig. 4 shows slight indications of particle p_t excesses in the forward tagging region, the number of events is small, and there is no clear evidence for a substantial third component, although one at the level of 15% of the QPM term is not excluded. Otherwise the GVDM+QPM model represents the data well, confirming the correctness of the fragmentation parameters used. This conclusion extends to the thrust and jet angle distributions, and was confirmed by examining distributions of kinematic variables. We estimate systematic errors in the tagged cross sections of 10% due to uncertainties in the reconstruction, tagger acceptance

and calibration.

The behaviour of the QPM term with Q^2 is fixed, but a number of possibilities exist for the hadronic term. We investigated the following:
(1) GVDM
(2) A vector meson dominance model consisting just of ρ, ω and ϕ poles.
(3) ρ-pole dominance alone (without the longitudinal term).
(4) The GLM model.
For each of models (1)–(3), we calculate the cross section of the hadronic term that is required to fit the total numbers of events observed in each tagging region. The Q^2 dependence of the model then gives in each case a value for the untagged hadronic cross section. The results are shown in table 3. At this stage, no third component was included in any of the models. The errors shown are statistical, and it is apparent that even if the 10% systematic errors are treated as random between the three Q^2 regions, only GVDM gives a consistent picture. The situation can be represented in terms of the ratio $R_{\gamma\gamma}$, defined as the ratio of the observed number of events to the number predicted by QPM in a given kinematic region. This is displayed in fig. 13 for the two-component models, showing how of these only GVDM gives a sufficiently slow fall-off with Q^2.

This conclusion is reinforced if the presence of a third component is taken into account. In the previous section it was established that this reduces the amount of GVDM required in the untagged data by approximately 20%. Similar effects are to be expected for models (2) and (3), since all three models behave similarly at low Q^2. If allowance is made for the possible presence of a small extra component in the forward tagged data, at the level of $15 \pm 15\%$ of the QPM cross section, the hadronic cross-sections in the second column would be reduced by $5 \pm 5\%$. Such corrections increase the consistency of the GVDM picture slightly, and make the other models worse.

The GLM model, with no free parameters, was also found to give a good description of the data over the whole W_{vis} and Q^2 range. Discrepancies of 5–10% were typically obtained, compatible with the systematic errors on the present measurements. This demonstrates the satisfactory nature of the model, and a good general agreement of our results with those of other experiments.

8. Conclusions

We have measured the production of multihadronic states by photon-photon interactions for visible final-state masses in the range 4–9 GeV, corresponding to true masses of typically 5–12 GeV. Results have been evaluated for untagged data (at mean $Q^2 \approx 0.03$ $(\mathrm{GeV/c})^2$), and at Q^2 values in ranges centred around 1 and 12 $(\mathrm{GeV/c})^2$. In the absence of a general theory of the process we have used a phenomenological model to describe our results. It was found that the data are well represented as an incoherent sum of Generalised Vector Meson Dominance and Quark Parton Model terms at the higher Q^2 values, using non-standard fragmentation for the GVDM term in agreement with that used by PLUTO. Agreement is also good for low-p_t tracks and jets over the whole Q^2 range. However, a third term is required at $Q^2 \simeq 0$ for events with $p_t^{jet} > 2$ GeV/c. A $1/W^2$ dependence is favoured for this term, the events having thrust intermediate between phase-space and QPM. The multijet models tested did not describe the transverse momentum distribution of these events in a plausible way, and a strongly enhanced charm contribution was not supported. The kind of term that appears to be suggested by the data would be a process with a QPM-like cross section, with broadening of the final-state

quark fragmentation by higher order effects.

The variation of the cross sections with Q^2 was described well by GVDM+QPM, and also by the GLM model, but poorly by simpler vector meson dominated models. These gave too rapid a fall-off with Q^2. At the highest Q^2 values, as found by other experiments, the quark parton model alone accounted for the majority of the cross section, confirming an interpretation of the process as becoming increasingly point-like in nature.

The GVDM component of the cross section at Q^2=0 was consistent with being flat in W, with a value of 200 ± 20 nb if a third component is included in the fit, or 250 ± 25 nb if it is excluded. This is consistent with the figure of 232 ± 15 nb. obtained by PLUTO without the inclusion of a third component. It disagrees with the results of TPC/2γ [3], who quote a value of $416 \pm 26 \pm 46$ nb. The magnitude of the third component required at Q^2=0 is also consistent with the result of PLUTO.

Acknowledgements.

We gratefully acknowledge the outstanding efforts of the PETRA machine group which made possible these measurements. We are indebted to the DESY computer centre for their excellent support during the experiment. We acknowledge the invaluable effort of the many engineers and technicians from the collaborating institutions in the construction and maintenance of the apparatus. The visiting groups wish to thank the DESY Directorate for the support and kind hospitality extended to them. This work was partly supported by the Bundesministerium für Forschung und Technologie (Germany), the Commissariat à l' Energie Atomique and the Institut National de Physique Nucléaire et de Physique des Particules (France), the Istituto Nazionale di Fisica Nucleare (Italy), the Science and Engineering Research Council (UK) and the Ministry of Science and Development (Israel).

References

[1] PLUTO Collaboration, Ch. Berger et al., Z. Phys. **26C** (1984) 191; Z. Phys. **26C** (1984) 353; Phys. Lett. **149B** (1984) 421
[2] PLUTO Collaboration, Ch. Berger et al., Z. Phys. **33C** (1987) 351
[3] TPC/2γ Collaboration, H. Aihara et al., Phys. Rev. **41D** (1990) 2667
[4] E. Gotsman, A. Levy, and U. Maor, Z. Phys. **40C** (1988) 117
[5] V. M. Budnev et al., Phys. Rep. **15C** (1975) 181
[6] K. Kajantie and R. Raitio, Phys. Lett. **87B** (1979) 133; R. N. Cahn and J. F. Gunion, Phys. Rev. **D20** (1979) 2753
[7] S. J. Brodsky and G. R. Farrar, Phys. Rev. Lett. **31** (1973) 1153; Phys. Rev. **D11** (1975) 1309; S. J. Brodsky et al., Phys. Rev. **D19** (1979) 1418; see also K. Kajantie, Acta Physica Austriaca, Suppl. XXI (1979) 633.
[8] F. J. Berends, P. H. Daverveldt and R. Kleiss, Z. Phys. **22C** (1984) 239
[9] H. J. Behrend et al., Physica Scripta **23** (1981) 610
[10] TASSO Collaboration, W. Braunschweig et al., Z. Phys. **C47** (1990) 499
[11] TPC/2γ Collaboration, M. Alston-Garnjost et al., Phys. Lett. **B252** (1990) 499

Tagging region	Q^2 range $(\mathrm{GeV/c})^2$	$< Q^2 >$	Data	Background
Untagged	0.–0.3	0.1	15610	1859
Forward	0.6–1.8	1.0	371	30
Endcap	4–28	12.7	302	54

Table 1: Final numbers of events. The numbers of data events include the background.

Third component	$\chi^2/d.f.$ Thrust	$\chi^2/d.f.$ p_t^{jet}	$\chi^2/d.f.$ W_{vis}	GVDM	QPM	Phase space	σ(GVDM) (nb)
none	16.9	37.7	16.6	11386	2364	0	252
(1)	6.6	3.4	2.9	8767	4983	0	194
(2a)	9.8	7.3	5.0	9906	2364	1480	219
(2b)	9.3	3.5	2.7	9450	2364	1936	209

Table 2: Parameters for best fits to the p_t^{jet} distribution of the untagged data. The models are described in the text. The columns for W_{vis} and thrust refer to the 1480 events selected with $p_t^{jet} > 2$ GeV/c.

Process	Untagged	Forward tag	Endcap tag
GVDM	252±2	229±16	225±26
VMD	264±2	341±24	633±73
ρ-pole	271±2	498±35	2982±343

Table 3: Cross sections in nb for the hadronic component at Q^2=0 required to fit the measured data at varying Q^2 using the models quoted. No third component is included in the fit of the untagged data. Errors are statistical only.

Figure Captions.

1. Feynman diagram for the process $\gamma\gamma \to q\bar{q}$.
2. Numbers of accepted events per GeV with given visible mass W_{vis}, compared with the calculated annihilation background.
3. W_{vis} distributions (events / 0.5 GeV) after background subtraction for (a) untagged, (b) forward tagged, (c) endcap tagged events.
4. Inclusive particle p_t distributions for the three Q^2 ranges (events / 0.5 GeV/c), compared with GVDM+QPM (dashed) and QPM alone (dotted).
5. p_t^{jet} distributions for the three Q^2 ranges (events / 0.5 GeV/c), compared with GVDM+QPM.
6. The angle θ^{jet} between the reconstructed jet axis and the $\gamma\gamma$ axis for the three Q^2 ranges (events / 10 degrees), compared with GVDM+QPM (dashed) and QPM alone (dotted).
7. p_t^{jet} distributions for the three Q^2 ranges (events / 0.5 GeV/c), compared with GVDM (dashed) and QPM (dotted) separately.
8. Inclusive particle p_t, p_t^{jet} and θ^{jet} distributions for untagged events, compared with GVDM + renormalised QPM.
9. Thrust distributions for the three Q^2 ranges (events / 0.05 unit), compared with GVDM+QPM.
10. As fig. 9 for events with $p_t^{jet} > 2$ GeV.
11. As fig. 10 compared with (a) GVDM+QPM + phase space, (b) GVDM + renormalised QPM.
12. Q^2 distributions (events / 0.5 (GeV/c)^2) for (a) forward, (b) endcap tagged regions compared with GVDM+QPM (dashed) and QPM alone (dashed-dotted).
13. $R_{\gamma\gamma}$ ratio at mean Q^2 value of each region. Solid squares = data; o=GVDM+QPM; ×=VMD+QPM; Δ=ρ-pole+QPM; +=GLM (QPM term included). The GLM point at the lowest (untagged) Q^2 value is a fixed prediction; the other models are all normalised to the data at this point.

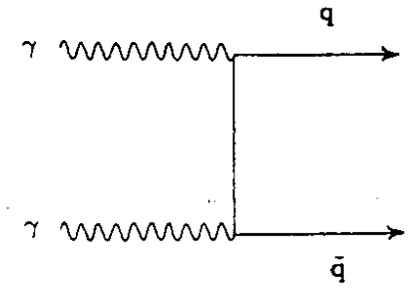

Fig. 1

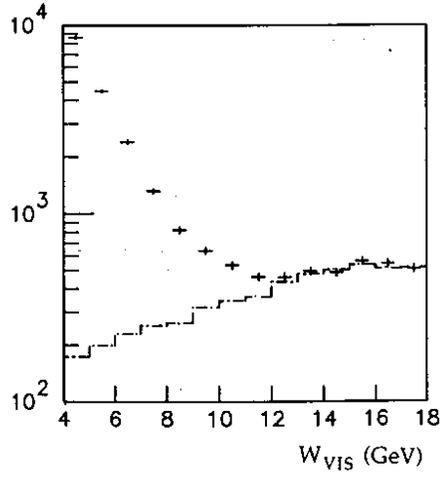

Fig. 2

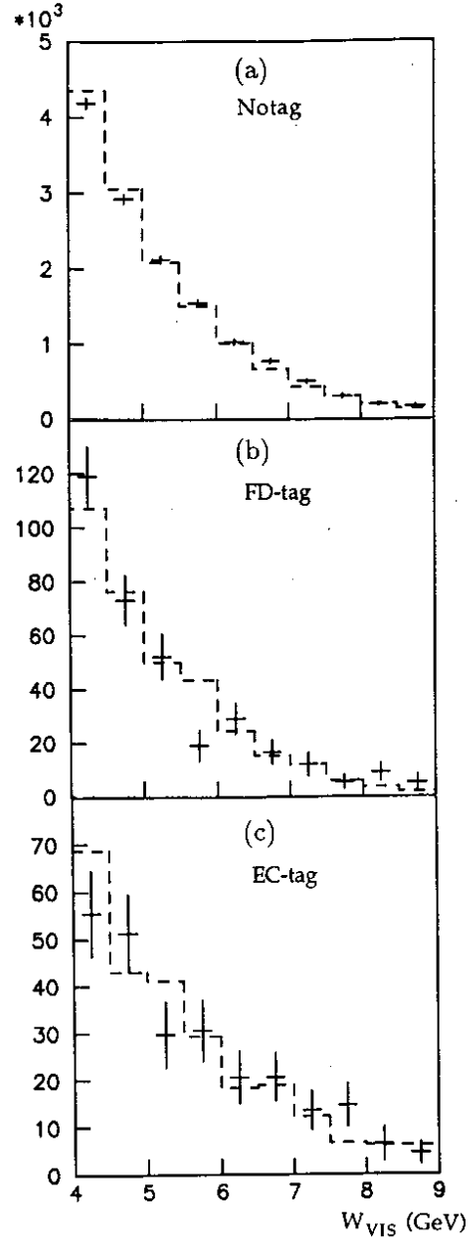

Fig. 3

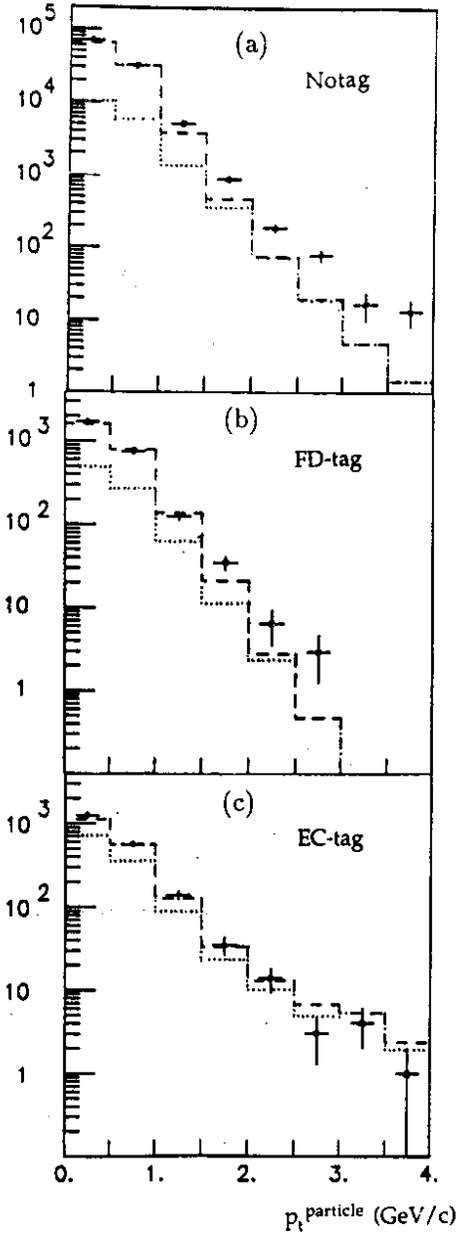

Fig. 4

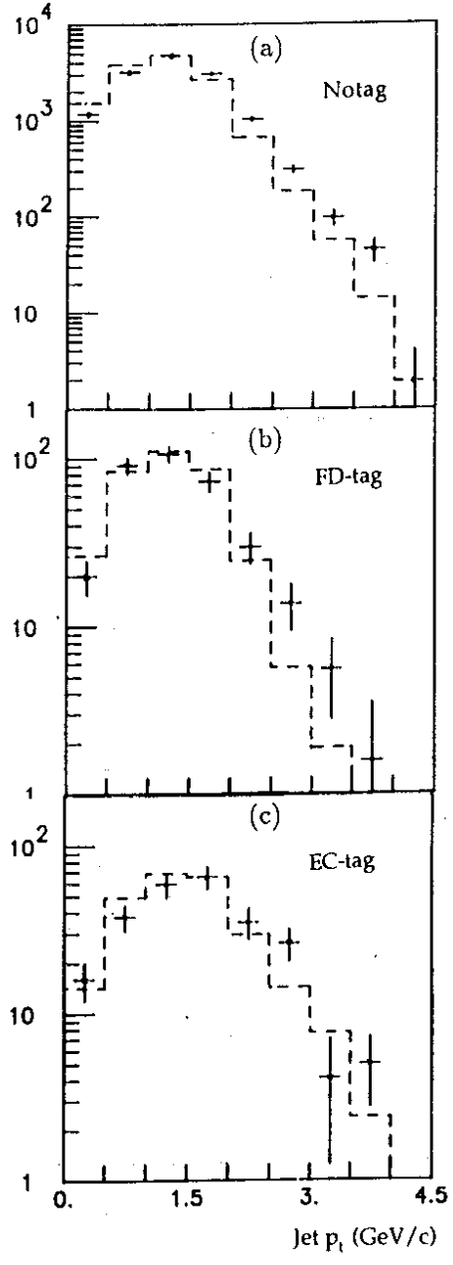

Fig. 5

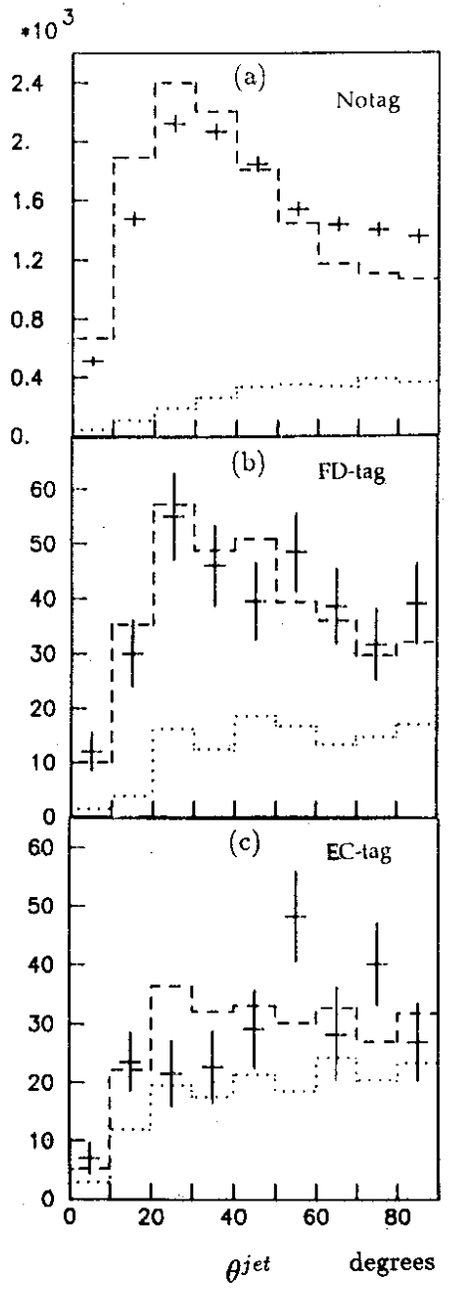

Fig. 6

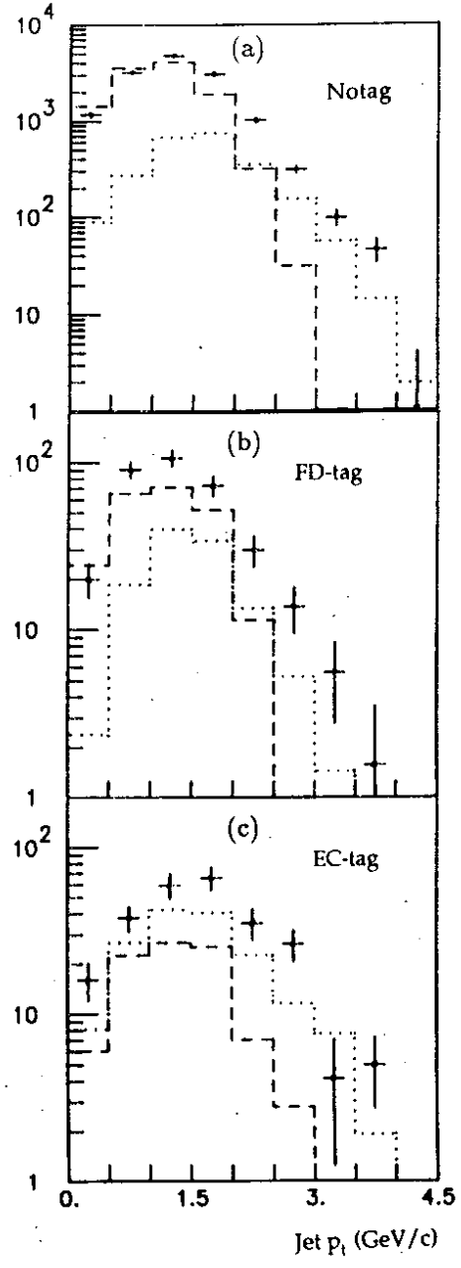

Fig. 7

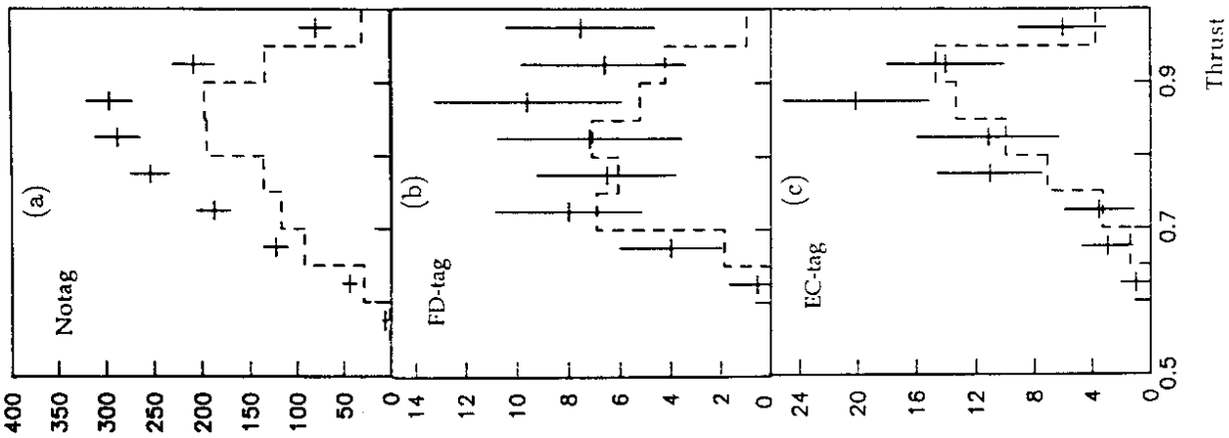

Fig. 10

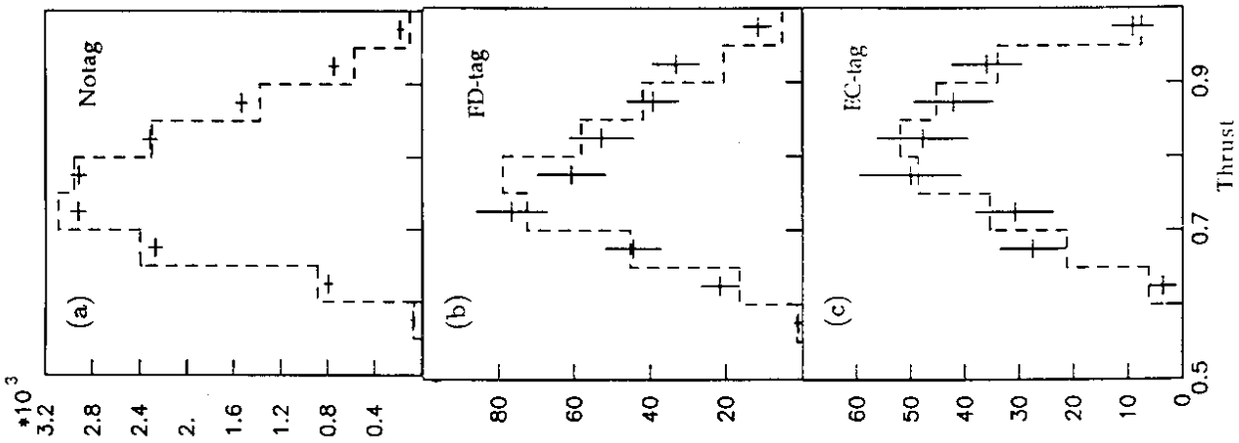

Fig. 9

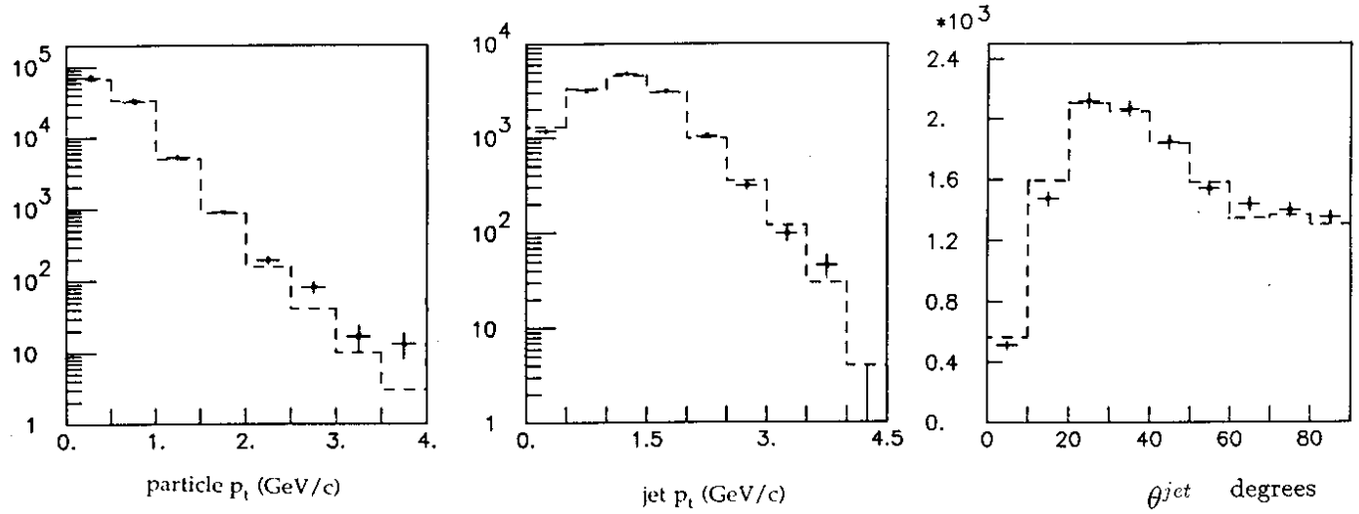

Fig. 8

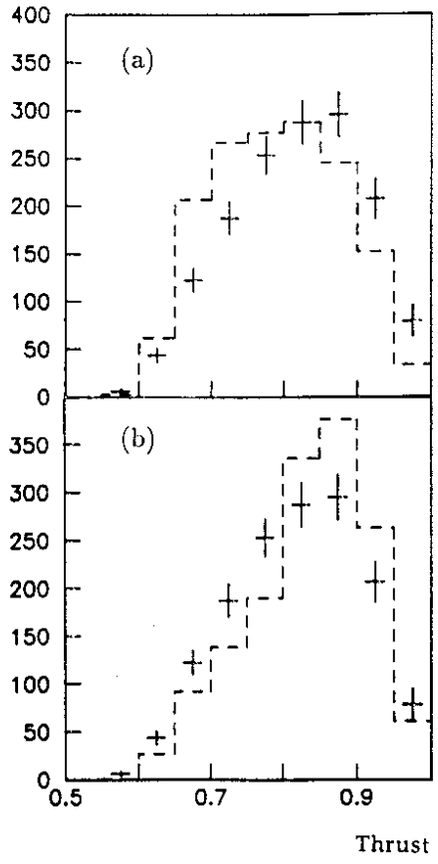

Fig. 11

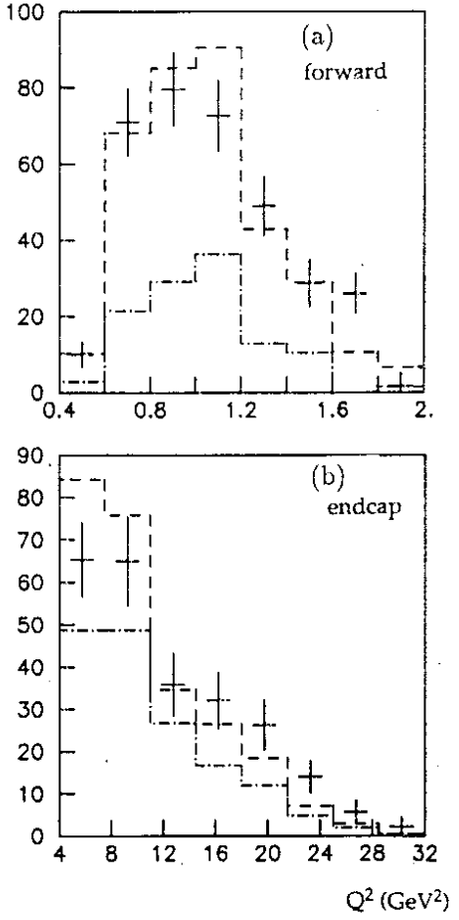

Fig. 12

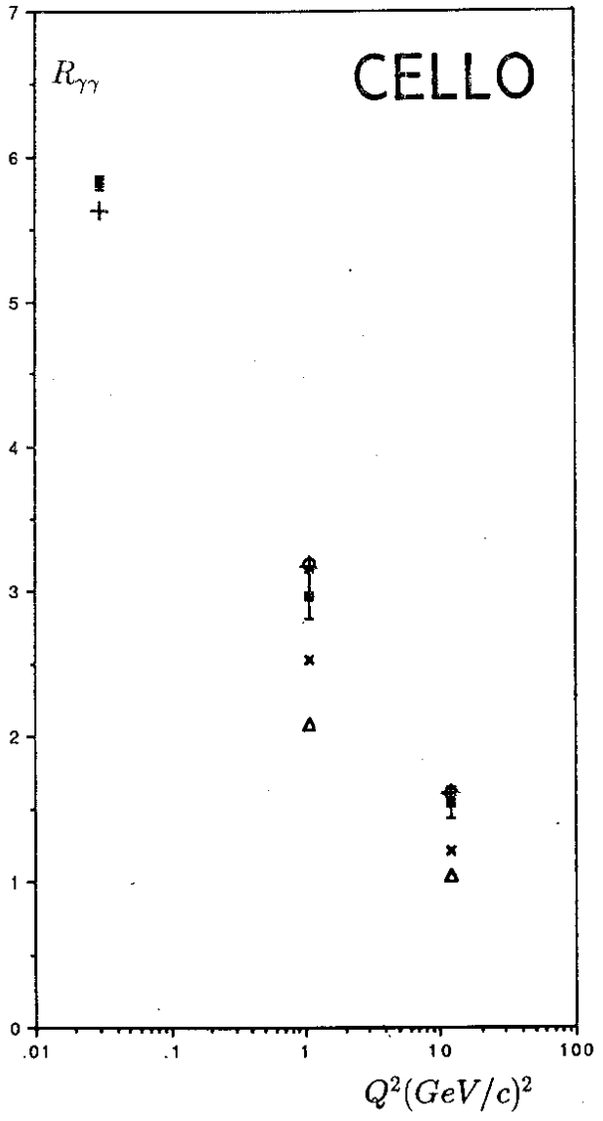

Fig. 13